# Unveiling Electronic Correlation and the Ferromagnetic Superexchange Mechanism in the van der Waals Crystal $CrSiTe_3$

Jiaxin Zhang,[1,§] Xiaochan Cai,[1,§] Wei Xia,[1] Aiji Liang,[1] Junwei Huang,[2] Chengwei Wang,[3,1] Lexian Yang,[4] Hongtao Yuan,[2] Yulin Chen,[1,4,5] Shilei Zhang,[1] Yanfeng Guo,[1,*] Zhongkai Liu,[1,†] and Gang Li[1,‡]

[1]*School of Physical Science and Technology, ShanghaiTech University, Shanghai 200031, China*

[2]*National Laboratory of Solid-State Microstructures, College of Engineering and Applied Sciences, and Collaborative Innovation Center of Advanced Microstructures, Nanjing University, Nanjing 210093, People's Republic of China*

[3]*Shanghai Institute of Microsystem and Information Technology, Chinese Academy of Sciences, Shanghai 200050, China*

[4]*State Key Laboratory of Low Dimensional Quantum Physics, Department of Physics, Tsinghua University, Beijing 100084, People's Republic of China*

[5]*Department of Physics, University of Oxford, Oxford OX1 3PU, United Kingdom*

(Received 25 August 2018; revised manuscript received 27 April 2019; published 23 July 2019)

The recent discovery of intrinsic ferromagnetic order in the atomically thin van der Waals crystal $CrXTe_3$ ($X$ = Si, Ge) stimulates intensive studies on the nature of low-dimensional magnetism because the presence of long-range magnetic order in two-dimensional systems with continuous symmetry is strictly prohibited by thermal fluctuations. By combining advanced many-body calculations with angle-resolved photoemission spectroscopy we investigate $CrSiTe_3$ single crystals and unveil the pivotal role played by the strong electronic correlations at both high- and low-temperature regimes. Above the Curie temperature ($T_c$), Coulomb repulsion ($U$) drives the system into a charge transfer insulating phase. In contrast, below $T_c$ the crystal field arranges the Cr-3$d$ orbitals such that the ferromagnetic superexchange profits, giving rise to the bulk ferromagnetic ground state with which the electronic correlations compete. The excellent agreement between theory and experiment establishes $CrSiTe_3$ as a prototype low-dimensional crystal with the cooperation and interplay of electronic correlation and ferromagnetism.

DOI: 10.1103/PhysRevLett.123.047203

*Introduction.*—The manipulation of long-range magnetic order in low-dimensional systems is an intriguing challenge holding great promise for future spintronic applications. Experimental progress over the past few years has made it possible to test the fundamental concept of magnetic correlations related to the motion of electrons in low dimensions. Recently, several van der Waals (vdW) materials (e.g., $CrGeTe_3$/$CrSiTe_3$, $CrI_3$/$CrBr_3$) have been found to host ferromagnetism (FM) down to the monolayer limit and to demonstrate a thickness dependence of their transition temperatures [1–6]. As spontaneous magnetization of uncompensated electron spins is hard to achieve particularly in the low dimension limit due to the Mermin-Wagner theorem [7], the experimental discovery of ferromagnetism in these vdW materials stimulates a renewed interest in low-dimensional magnetism.

An intriguing fact about these transition-metal compounds is that they are natural hosts of both electronic correlations and magnetism. Their interplay is often the source of many exotic phenomena, such as a Mott insulator [8,9], high temperature superconductivity [10–16] and colossal magnetoresistance [17,18]. After the successful demonstration of ferromagnetism, the nature of the charge insulating state and the FM coupling mechanism of these vdW materials were urged to be clarified. Furthermore, at low-temperature the strength of the spin-orbit coupling (SOC) inherited from Te-$p$ bands becomes comparable to the spin couplings. Thus, the presence of different competing degrees of freedom (d.o.f.), i.e., electronic correlation, magnetic superexchange and SOC, and their relations with the robustness of low-dimensional ferromagnetism poses a fundamental quest to be resolved.

In order to address this question, we grew high-quality $CrSiTe_3$ single crystal and performed high-resolution angle-resolved photoemission spectroscopy (ARPES). By performing systematic photon-energy and polarization dependence measurements we were able to identify the full set of electronic structure near the Fermi level. After comparing to the advanced many-body calculations, we reveal the correlated nature of $CrSiTe_3$ at both high and low-temperature regimes with the electronic structure further renormalized by the SOC. The excellent agreement between theory and experiment establishes $CrSiTe_3$ as a Mott-type FM insulator.

*Results.—A. Sample preparation and magnetic properties.*—$CrSiTe_3$ single crystals were synthesized using the flux method (see Supplemental Material for details [19]).

 

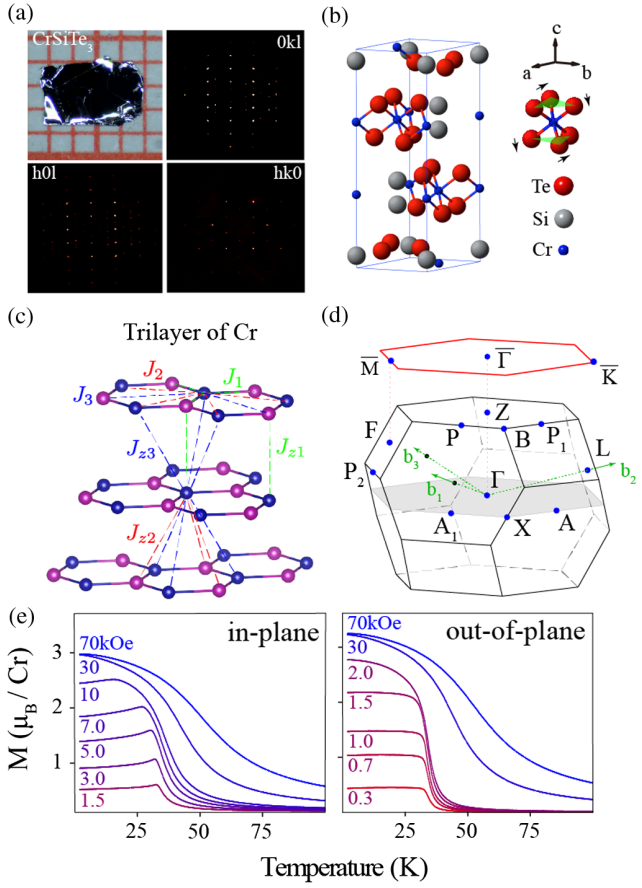


FIG. 1. Crystal structure and physical property of $CrSiTe_3$. (a) Photo of $CrSiTe_3$ single crystal and x-ray diffraction patterns, with indices of lattice planes labeled. (b) Unit cell of the crystal structure. Each Cr atom is surrounded by six Te atoms distorted along the directions indicated by the arrows. (c) In each unit cell, inequivalent Cr atoms form three layers of effective honeycomb stacking along the $c$ direction. The intralayer and interlayer spin couplings used in the effective Heisenberg model are illustrated as $J_1$, $J_2$, $J_3$, and $J_{z1}$, $J_{z2}$, $J_{z3}$, respectively. (d) The Brillouin zone (BZ) and the high symmetry points. The $k_z = 0$ plane intersects with the BZ boundary at arbitrary $k$ points. (e) Temperature dependent in-plane (left panel) and out-of-plane (right panel) magnetic moment per Cr atom under different magnetic fields.

The high quality of the crystal is verified by the x-ray diffraction (XRD) measurements shown in Fig. 1(a). The rhombohedral crystal structure of $CrSiTe_3$ is presented in Fig. 1(b). A Cr-Te form edge shared octahedron layer-stacking along the $c$ direction. Inside each layer, connecting nearest-neighbor Cr atoms gives rise to an effective honeycomb lattice which displaces its center from those of the layers above and below it as shown in Fig. 1(c). The six Te atoms around the central Cr atom form an octahedron which is slightly distorted along the direction indicated by the arrows in Fig. 1(b), making the local point symmetry, known as $D_{3d}$, slightly lower than cubic symmetry.

The magnetic nature is characterized by the temperature dependent magnetic susceptibility of bulk $CrSiTe_3$ under parallel (in-plane) and perpendicular (out-of-plane) magnetic field (with respect to the $a$-$b$ plane of the sample) with the field varying from 1.5 to 70 kOe [Fig. 1(e)]. As clearly visualized, a magnetic phase transition occurs at $T_c \sim 33$ K, which is consistent with other reports [30–32]. We notice the $\lambda$ shape in the susceptibility curve below $T_c$ with the in-plane field coming from the magnetic anisotropy and suggesting the FM points out of plane [33]. The layered $CrSiTe_3$ crystal could be easily cleaved along its (111) directions. To prepare clean $CrSiTe_3$ surfaces for surface sensitive x-ray photoelectron spectroscopy (XPS) and ARPES measurements, we cleaved the single crystal $CrSiTe_3$ inside the vacuum chamber prior to the measurements. After cleaving, XPS measurement shows the high quality of the sample by seeing the characteristic core level peaks from Cr, Si, and Te (see Fig. S1a in the Supplemental Material [19]) while the broad Fermi surface mapping (see Fig. S1c [19]) covering multiple BZs confirmed the (111) cleavage plane, which allows us to carry out the study below.

*B. High-temperature charge transfer insulating phase.*—Figure 2(a) (right) presents the electronic structure measured by ARPES in the paramagnetic (PM) phase. From the broad range dispersion along the $A_1$-Γ-$A$ direction [Fig. 2(a)(ii)] we could identify both dispersive feature (near the valence band maximum, or VBM and down to 6 eV below) and rather flat bands (~1.5 eV below the VBM). The dispersive features are found to be the $p$ orbitals of Te and Si while the flat features are coming from the Cr-$d$ bands. By performing photon-energy and polarization dependent measurement, we obtained the full 3D electronic structure of $CrSiTe_3$ shown in Figs. 2(b) and 2(c), where several holelike bands near the VBM were detected and one of them shifts 400 meV down when moving from the Γ to the $Z$ point (More details of the $k_z$ evolution could be found in SI.II [19]). The absence of spectral weight above the observed valence band top [as indicated by the integrated energy distribution curve plot by the side of Figs. 2(a)(ii) and 2(c)(i),(iv)] suggests the semiconducting or insulating nature of $CrSiTe_3$ in the PM phase. Further optical absorption measurement provides an indirect gap size ~0.4 eV and direct gap size ~1.2 eV [31,34]. Both experimental shreds of evidence suggest that, before the onset of long-range FM, electrons have been fully localized, which is in sharp contrast to first-principles calculations that will be discussed below.

In the absence of FM, $CrSiTe_3$ is predicted, by *ab initio* calculations, to be metal as evidenced by the bands crossing the Fermi level [Fig. S3(a)]. Inspecting the nonmagnetic electronic band structure where the energy bands are projected to Cr-$d$ orbitals under $D_{3d}$ crystal environment, we find the $d_{z^2}$ and $d_{x^2-y^2}$ distribute mainly at the Fermi level, while $d_{zx} + d_{yz}$ occupy also at the conduction bands between 1 and 2 eV. The Cr-$d$ bands, at the Fermi level, are confined in a narrow energy range within 1 eV, which strongly favors the interactions between electrons. Further,

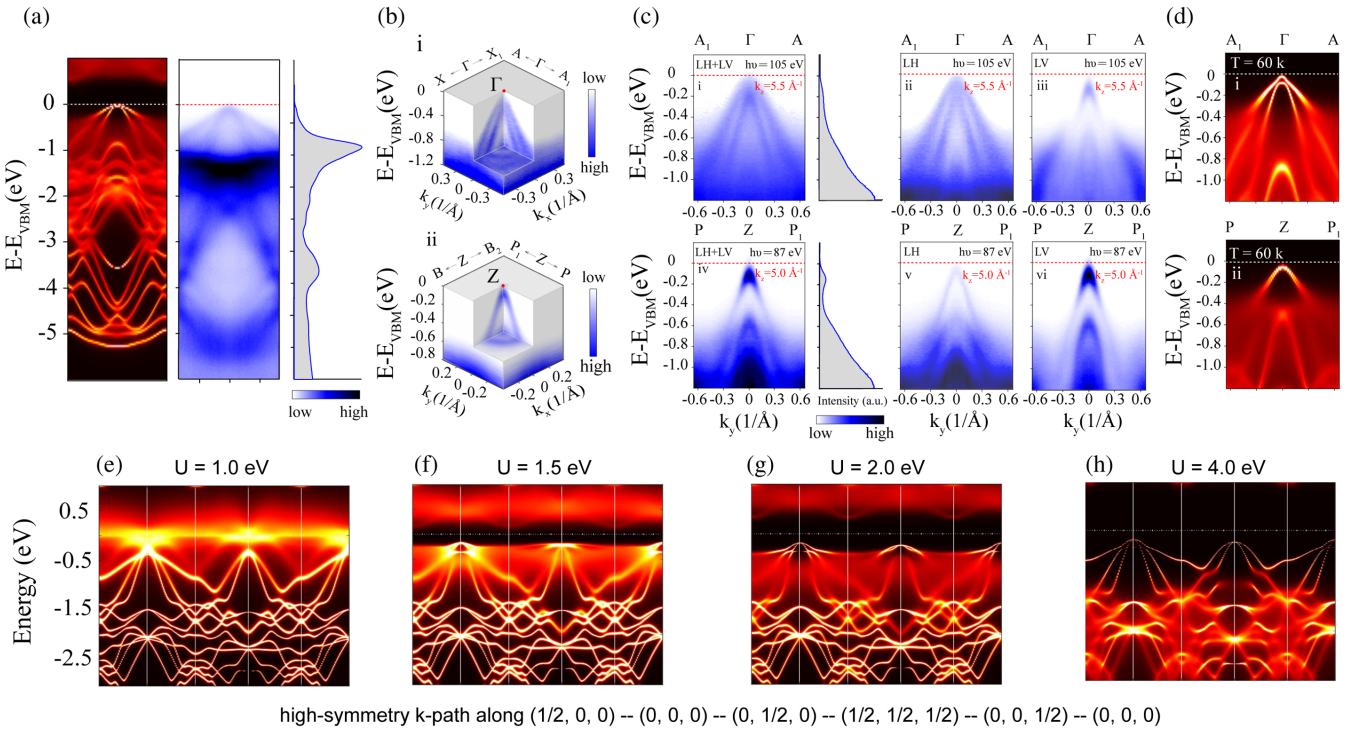


FIG. 2. Electronic band structure of paramagnetic $CrSiTe_3$. (a) The dispersion calculated with eDMFT + SOC at 60 K with $U = 4.0$ eV along $A_1$-Γ-$A$ $k$ path (i) and the corresponding ARPES measurement at 200 K (ii). (b) Three-dimensional electronic structure measured at the Γ (i) and $Z$ (ii) points. (c) High symmetry cuts along the $A_1$-Γ-$A$ direction measured with linear horizontal (ii) and linear vertical (iii) polarized photons, and their superposition (i). (iv)–(vi) Same as (i)–(iii), but along the $P$-$Z$-$P_1$ direction. Data of (b) and (c) are measured at room temperature. (d) The calculated band structure from eDMFT + SOC around Γ and $Z$ in the energy range, same as in (c). (e)–(h). Correlated spectra of $CrSiTe_3$ calculated by eDMFT with different $U$ value at 230 K, i.e., (e) 1.0, (f) 1.5, (g) 2.0, and (h) 4.0 eV. In these calculations SOC is neglected for simplicity.

given the fact that the valence electrons of Cr-ion are in their $d^3$ configuration and there are 3 bands/Cr-ion occupied [we note the saturated magnetic moment is close to 3 $\mu B$/Cr, see Fig. 1(e)], the two necessary ingredients for the Mott transition are both satisfied, i.e., the strong Coulomb interactions from the narrow $d$ bands and the half-filled condition. The insulating states at high temperature are, thus, likely to be a Mott state.

To investigate this hypothesis and to characterize the nature of the high-temperature charge gap, we employed the DFT + dynamical mean-field theory (DMFT) as implemented in the embedded-DMFT package [35] to account for the local Coulomb interactions between the Cr-$d$ electrons (see details of the eDMFT calculations in SI.III [19]). As shown in Figs. 2(e)–2(h), as a function of $U$, the correlated spectra of $CrSiTe_3$ gradually loses its weight at the Fermi level and a charge gap opens at the $U$ value between 1.0 and 1.5 eV. Upon further increasing $U$ values, the correlated Cr-$d$ bands pass through the dispersive valence $p$ bands and move further to high energies. The low-energy $p$ bands are less influenced by the renormalization of Cr-$d$ bands as the $p$-$d$ hybridization is not strong in this system evidenced from the Wannier orbital plot shown in the Supplemental Material, Fig. S4, where the projected orbitals nicely preserve their atomic symmetries [19]. We note that, though immune to electronic correlations, the low-energy $p$ bands can be strongly modified by SOC. The cooperation of interaction and SOC included in an eDMFT + SOC calculation significantly changes the upper valence bands, resulting in a nice agreement with the ARPES measured electronic structure [see Figs. 2(a), 2(c), and 2(d) for comparison].

Based on the experiment-theory agreement, we conclude that the high-temperature $CrSiTe_3$ can be driven into a gapped phase solely by electronic correlations; i.e., no assistance from the long-range magnetic order is needed. However, the possible influence of short-range magnetic correlations cannot be excluded by our calculations. They are found to persist to 150 K in $CrSiTe_3$ [5,36], i.e., a temperature much higher than Curie temperature $T_c$. The charge gap is likely to result from the interplay of short-range magnetic correlations and electronic interactions, while our many-body calculations show that the nature of the charge gap is essentially determined by the correlation.

*C. Mechanism of low-temperature ferromagnetic coupling.*—We further elaborate on the low-temperature FM phase by studying the nature of the magnetic coupling. With the decreasing of temperature and the localization of the electrons, the charge d.o.f. become less active due to the formation of the energy gap. Meanwhile, the spin d.o.f.

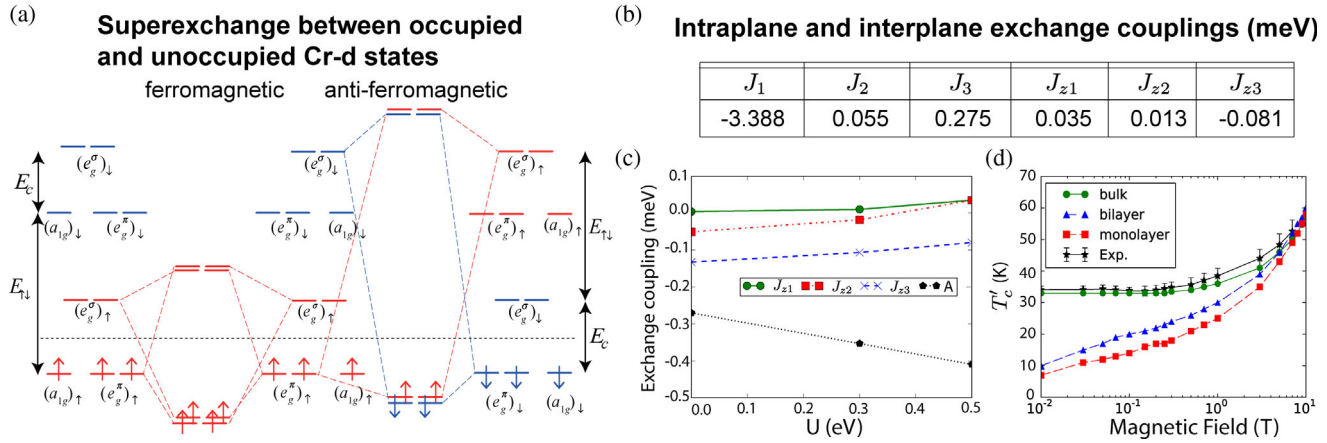


| $J_1$ | $J_2$ | $J_3$ | $J_{z1}$ | $J_{z2}$ | $J_{z3}$ |
|---|---|---|---|---|---|
| -3.388 | 0.055 | 0.275 | 0.035 | 0.013 | -0.081 |

FIG. 3. (a) Superexchange process favouring the ferromagnetic coupling of the Cr local moments. (b) The value of exchange couplings determined for bulk $CrSiTe_3$. (c) The interlayer exchange couplings $J_{z1}, J_{z2}, J_{z3}$, and magnetic anisotropy strength $A$ are sensitive to the choice of $U$ parameters, which become antiferromagnetic with the increase of $U$ value. However, the magnetic anisotropy $A$ is enhanced with larger interactions. (d) The predicted transition temperatures $T_c'$ under external magnetic field. Here the bulk exchange coupling parameters are used in monolayer and bilayer calculations; the obtained transition temperature decreases with the reduction of layer thickness.

come into play. First, it is clear that the FM coupling between Cr local magnetic moments is indirect, because $T_c$ is much larger in $CrGeTe_3$ (~67 K) than in $CrSiTe_3$ (~33 K) despite, in the former, the distance between two neighboring Cr atoms is larger. Second, we identify two different superexchange processes, i.e., the exchange of $a_{1g} + e_g^\pi$ states with $a_{1g} + e_g^\pi$ and $e_g^\sigma$ states, respectively. Here $a_{1g}$ and $e_g^\pi$ are the half-filled singlet and doublet states, while $e_g^\sigma$ is the unoccupied doublet state. Only the exchange of $a_{1g} + e_g^\pi$ states with $e_g^\sigma$ states leads to a ferromagnetic coupling between the Cr neighboring local moments. The energy levels of $a_{1g} + e_g^\pi$ and $e_g^\sigma$ states, after taking hybridization into account, are plotted in Fig. 3(a). If the two neighboring local moments are FM coupled, the lowest energy levels are given by the bonding states between the $e_g^\pi$ and $e_g^\sigma$ states with the same spin projections. Given the hybridization strength $\Delta$, four of the six electrons at two neighboring Cr atoms will stay at lower energy levels $-6\Delta^2/E_c$ with $E_c$ being the strength of crystal field splitting. The two remaining $a_{1g}$ electrons do not participate in this superexchange process. Otherwise, if the local moments are AFM coupled, the bonding states between neighboring $e_g^\pi$ and $e_g^\sigma$ states only gain smaller energy reduction $-6\Delta^2/(E_c + E_{\uparrow\downarrow})$, where $E_{\uparrow\downarrow}$ is the spin polarization amplitude. Consistent with the Goodenough-Kanamori rule [37,38], we conclude that, in addition to the magnetic anisotropy, the long-range FM in $CrSiTe_3$ is mainly derived from the superexchange between the $e_g^\pi$ and $e_g^\sigma$ states, which is strongly competed with by the AFM coupling resulting from $e_g^\pi$ and $e_g^\pi$ exchange (see Supplemental Material, Fig. S6 for more details [19]).

After clearly demonstrating the high-temperature correlated phase and the low-temperature FM superexchange mechanism, we want to further discuss the competition of electronic correlations with the long-range FM order. Figure 3(b) lists the calculated spin coupling strengths by employing the four-states method [39] within *Dudarev*'s DFT + $U$ scheme [40]. Compared to the values reported for $CrGeTe_3$ [1], the absolute values of all couplings are reduced in $CrSiTe_3$, with only the nearest neighbor coupling $J_1$ remaining ferromagnetic. Others become essentially antiferromagnetic. Furthermore, we find that these couplings are sensitive to the value of Coulomb interactions. All three interlayer couplings increase towards AFM with the increase of $U$ as shown in Fig. 3(c). Further increasing $U$ $CrSiTe_3$ transforms from FM to a new magnetic state with FM intralayer coupling and AFM interlayer coupling. The strong competition between electronic Coulomb interaction and magnetic superexchange coupling, in particular at low-dimensions with an enhanced electronic repulsion, may generate larger magnetic anisotropy, leading to the emergence of new magnetic states and increased transition temperatures [41].

With the obtained bulk exchange coupling strength, following Ref. [1] we further calculate the transition temperature $T_c'$ of $CrSiTe_3$ by solving the Heisenberg model with linear spin wave theory under the out-of-plane magnetic field. With finite magnetic field, the transition temperature $T_c'$ is no longer the Curie temperature defined for the ferromagnetic phase transition. Nevertheless, it similarly defines the temperature above which the calculated magnetic moment drops to zero. $T_c'$ for the bulk, bilayer, and monolayer $CrSiTe_3$ are shown in Fig. 3(d), which monotonically decreases with the decrease of magnetic field strength. As for bulk $CrSiTe_3$, a constant value at low field and a linear dependence on $B$ of $T_c'$ at high field are observed, which is highly consistent with the

measurement and, on the other hand, validates the theoretically obtained exchange coupling parameters shown in Fig. 3(b). In sharp contrast to the bulk case, bilayer and monolayer $CrSiTe_3$ display a magnetic field dependence of $T_c'$ even at the low field limit. Thus, the low-dimensional $CrSiTe_3$ is more tunable by an external magnetic field.

*Discussions.*—The interplay of charge and spin d.o.f. is one of the fascinating mechanisms that has triggered many novel phenomena in many-body systems. Though both electronic correlations and magnetic ordering can drive MIT individually, they often coexist in transition-metal compounds, which makes the nature of the insulating gap hard to interpret. It is then highly interesting to see in $CrSiTe_3$, especially at temperatures above $T_c$, the two mechanisms are nicely separated, which allows us to characterize the nature of the charge gap. The narrow Cr-*d* bands around the Fermi level are strongly correlated leading to the Mott insulating phase above the Curie temperature. At the low-temperature regime, the charge d.o.f. give their way to the spin d.o.f. due to the formation of charge gap. The specific electronic structure is found to strongly favor the superexchange coupling between the $e_g^\pi$ and $e_g^\sigma$ states, leading to the ferromagnetic ground states of bulk $CrSiTe_3$. Compared to $CrGeTe_3$, the strong competition from electronic correlations significantly weakens the interlayer ferromagnetic coupling, making $CrSiTe_3$ a system residing at the border of FM and *A*-type AFM (i.e., intralayer ferromagnetic and interlayer antiferromagnetic) that waits for further experimental verification. The discovered correlated nature of $CrSiTe_3$ greatly enriches our understanding of low-dimensional magnetism and may provide a new engineering parameter to achieve high-$T_c$ 2D magnetism.

This work is supported by grant from the National Key R&D program of China (Grant No. 2017YFA0305400) and Chinese Academy of Science-Shanghai Science Research Center (Grant No. CAS-SSRC-YH-2015-01). G. L., Z. L., and Y. G. acknowledge the starting grant of ShanghaiTech University. Y. G. and G. L. acknowledge the Program for Professor of Special Appointment (Shanghai Eastern Scholar). Z. L. and G. L. acknowledge the support from the National Natural Science Foundation of China (Grants No. 11674229 and No. 11874263). Calculations were carried out at the HPC Platform of ShanghaiTech University Library and Information Services, as well as School of Physical Science and Technology. ARPES measurements at DLS were under the Proposal No. SI18382. The authors greatly thank the Instrument Analysis Center of ShanghaiTech University.

*guoyf@shanghaitech.edu.cn
†liuzhk@shanghaitech.edu.cn
‡ligang@shanghaitech.edu.cn
§These authors contributed equally to this work.

[1] C. Gong, L. Li, Z. Li, H. Ji, A. Stern, Y. Xia, T. Cao, W. Bao, C. Wang, Y. Wang, Z. Qiu, R. Cava, S. G. Louie, J. Xia, and X. Zhang, Nature (London) **546**, 265 (2017).
[2] B. Huang, G. Clark, E. Navarro-Moratalla, D. R. Klein, R. Cheng, K. L. Seyler, D. Zhong, E. Schmidgall, M. A. McGuire, D. H. Cobden, W. Yao, D. Xiao, P. Jarillo-Herrero, and X. Xu, Nature (London) **546**, 270 (2017).
[3] Y. Liu and C. Petrovic, Phys. Rev. B **96**, 054406 (2017).
[4] G. T. Lin, H. L. Zhuang, X. Luo, B. J. Liu, F. C. Chen, J. Yan, Y. Sun, J. Zhou, W. J. Lu, P. Tong, Z. G. Sheng, Z. Qu, W. H. Song, X. B. Zhu, and Y. P. Sun, Phys. Rev. B **95**, 245212 (2017).
[5] B. Liu, Y. Zou, L. Zhang, S. Zhou, Z. Wang, W. Wang, Z. Qu, and Y. Zhang, Sci. Rep. **6**, 33873 (2016).
[6] M. Lin, H. L. Zhuang, J. Yan, T. Ward, A. A. Puretzky, C. M. Rouleau, Z. Gai, L. Liang, V. Meunier, B. G. Sumpter, P. Ganesh, P. R. Kent, D. B. Geohegan, D. G. Mandrus, and K. Xiao, J. Mater. Chem. C **4**, 315 (2015).
[7] N. D. Mermin and H. Wagner, Phys. Rev. Lett. **17**, 1133 (1966).
[8] N. F. Mott, Rev. Mod. Phys. **40**, 677 (1968).
[9] M. Imada, A. Fujimori, and Y. Tokura, Rev. Mod. Phys. **70**, 1039 (1998).
[10] E. Dagotto, Rev. Mod. Phys. **66**, 763 (1994).
[11] N. Mathur, F. Grosche, S. Julian, I. Walker, D. Freye, R. Haselwimmer, and G. Lonzarich, Nature (London) **394**, 39 (1998).
[12] T. Timusk and B. Statt, Rep. Prog. Phys. **62**, 61 (1999).
[13] Y. Maeno, H. Hashimoto, K. Yoshida, S. Nishizaki, T. Fujita, J. G. Bednorz, and F. Lichtenberg, Nature (London) **372**, 532 (1994).
[14] P. A. Lee, N. Nagaosa, and X.-G. Wen, Rev. Mod. Phys. **78**, 17 (2006).
[15] Y. Guo, Y. F. Zhang, X. Y. Bao, T. Z. Han, Z. Tang, L. X. Zhang, W. G. Zhu, E. Wang, Q. Niu, Z. Qiu, J. F. Jia, Z. X. Zhao, and Q. K. Xue, Science **306**, 1915 (2004).
[16] D. Scalapino, J. Low Temp. Phys. **117**, 179 (1999).
[17] Y. Tokura and Y. Tomioka, J. Magn. Magn. Mater. **200**, 1 (1999).
[18] A. Ramirez, J. Phys. Condens. Matter **9**, 8171 (1997).
[19] See Supplemental Material at http://link.aps.org/supplemental/10.1103/PhysRevLett.123.047203 for details of material growth, the $k_z$ dependence of ARPES, and many-body calculations, which includes Refs. [20–29].
[20] P. Hohenberg and W. Kohn, Phys. Rev. **136**, B864 (1964).
[21] W. Kohn and L. Sham, Phys. Rev. **140**, A1133 (1965).
[22] G. Kresse and J. Furthmüller, Phys. Rev. B **54**, 11169 (1996).
[23] P. E. Blöchl, Phys. Rev. B **50**, 17953 (1994).
[24] J. P. Perdew, K. Burke, and M. Ernzerhof, Phys. Rev. Lett. **77**, 3865 (1996).
[25] P. Blaha, K. Schwarz, G. K. H. Madsen, D. Kvasnicka, J. Luitz, R. Laskowski, F. Tran, and L. D. Marks, *WIEN2k, An Augmented Plane Wave + Local Orbitals Program for Calculating Crystal Properties* (Techn. Universität Wien, Austria, 2018), ISBN 3-9501031-1-2.
[26] P. Werner, A. Comanac, L. de Medici, M. Troyer, and A. J. Millis, Phys. Rev. Lett. **97**, 076405 (2006).
[27] P. Werner and A. J. Millis, Phys. Rev. B **74**, 155107 (2006).
[28] K. Haule, Phys. Rev. B **75**, 155113 (2007).

[29] E. Gull, A. J. Millis, A. I. Lichtenstein, A. N. Rubtsov, M. Troyer, and P. Werner, Rev. Mod. Phys. **83**, 349 (2011).
[30] G. Ouvrard, E. Sandre, and R. Brec, J. Solid State Chem. **73**, 27 (1988).
[31] L. Casto, A. Clune, M. Yokosuk, J. Musfeldt, T. Williams, H. Zhuang, M. Lin, K. Xiao, R. Hennig, B. Sales, J. Yan, and D. Mandrus, APL Mater. **3**, 041515 (2015).
[32] V. Carteaux, G. Ouvrard, J. Grenier, and Y. Laligant, J. Magn. Magn. Mater. **94**, 127 (1991).
[33] V. Carteaux, F. Moussa, and M. Spiesser, Europhys. Lett. **29**, 251 (1995).
[34] H. Ji, R. Stokes, L. Alegria, E. Blomberg, M. Tanatar, A. Reijnders, L. Schoop, T. Liang, R. Prozorov, K. Burch, N. Ong, J. Petta, and R. Cava, J. Appl. Phys. **114**, 114907 (2013).
[35] K. Haule, C.-H. Yee, and K. Kim, Phys. Rev. B **81**, 195107 (2010).
[36] T. J. Williams, A. A. Aczel, M. D. Lumsden, S. E. Nagler, M. B. Stone, J.-Q. Yan, and D. Mandrus, Phys. Rev. B **92**, 144404 (2015).
[37] J. Kanamori, J. Phys. Chem. Solids **10**, 87 (1959).
[38] H. Weihe and H. U. Güdel, Inorg. Chem. **36**, 3632 (1997).
[39] H. J. Xiang, E. J. Kan, S.-H. Wei, M.-H. Whangbo, and X. G. Gong, Phys. Rev. B **84**, 224429 (2011).
[40] S. L. Dudarev, G. A. Botton, S. Y. Savrasov, C. J. Humphreys, and A. P. Sutton, Phys. Rev. B **57**, 1505 (1998).
[41] N. Sivadas, M. W. Daniels, R. H. Swendsen, S. Okamoto, and D. Xiao, Phys. Rev. B **91**, 235425 (2015).